Novel Mixed-Mode Phase Transition Involving a Composition-Dependent Displacive Component

S. Nag,[1,2] A. Devaraj,[1] R. Srinivasan,[3] R. E. A. Williams,[4,5] N. Gupta,[1] G. B. Viswanathan,[6] J. S. Tiley,[6] S. Banerjee,[7] S. G. Srinivasan,[1,*] H. L. Fraser,[4,5] and R. Banerjee[1,2,†]

[1]*Department of Materials Science and Engineering, University of North Texas, Denton, Texas 76203, USA*
[2]*Center for Advanced Research and Technology, University of North Texas, Denton, Texas 76203, USA*
[3]*ExxonMobil Research and Engineering Company, Annandale, New Jersey 08801, USA*
[4]*Department of Materials Science and Engineering, The Ohio State University, Columbus, Ohio 43210, USA*
[5]*Center for Accelerated Maturation of Materials, The Ohio State University, Columbus, Ohio 43210, USA*
[6]*Materials and Manufacturing Directorate, Air Force Research Laboratory, Dayton, Ohio 45433, USA*
[7]*Department of Atomic Energy and Atomic Energy Commission, Mumbai, India*

(Received 8 March 2011; revised manuscript received 3 May 2011; published 17 June 2011)

Solid-solid displacive, structural phase transformations typically undergo a discrete structural change from a parent to a product phase. Coupling electron microscopy, three-dimensional atom probe, and first-principles computations, we present the first direct evidence of a novel mechanism for a coupled diffusional-displacive transformation in titanium-molybdenum alloys wherein the displacive component in the product phase changes continuously with changing composition. These results have implications for other transformations and cannot be explained by conventional theories.

DOI: 10.1103/PhysRevLett.106.245701 PACS numbers: 64.70.K−, 61.66.Dk, 68.37.Ef, 68.37.Hk

Solid-solid phase transformations are ubiquitous in nature and fundamental to modern materials science. The so-called first-order transformations involve discrete nucleation and growth of the product phase in the parent phase matrix, while second- (or higher) order ones involve a homogeneous continuous transformation from the parent to the product phases. Importantly, classical nucleation theory of first-order transformations assume that the second phase nucleus has the equilibrium composition and crystal structure of the product phase. The first-order transformations are further classified as diffusional, displacive, and coupled diffusional-displacive (mixed-mode) depending on the operative transformation mechanism. Mixed-mode transformations, such as the classical bainite transformation in steels, typically include coupled diffusional and displacive (often shear or shuffle-based) components. The bainite transformation in the Fe-C system involves decomposition of a face-centered cubic (fcc) parent phase (γ) into a body-centered cubic (bcc) α and orthorhombic cementite (Fe_3C) phases via diffusive partitioning of carbon followed by a displacive change in crystal structure. Importantly, this γ to α and similar first-order transformations are believed to involve a single discrete step over an activation energy barrier. This Letter, for the first time, presents evidence for a new mixed-mode solid-solid transformation wherein both a diffusive compositional change and a displacive structural change occur in a coupled yet continuous fashion, thus displaying features of a continuous solid-solid transformation while still being a first-order transformation. The newly discovered features include a partially collapsed intermediate structure lying in between parent and product phases and a composition-dependent displacive component of transformation (i.e., extent of collapse within the embryos). Our proposed mechanism explains the observed partially transformed embryos, lying in between the two end states, with local minima in the free energy landscape of the system.

This new transformation mechanism has been observed for the bcc (β) to the hexagonal ω phase transformation, directly relevant to a wide variety of important engineering alloys involving group IV elements. At ambient pressure, titanium (Ti), zirconium (Zr), hafnium (Hf), and other group IV elements exhibit two distinct allotriomorphs—stable low temperature hexagonal close-packed (hcp) α and stable higher temperature bcc β phases. Alloys of these elements, containing a critical concentration of β-stabilizing elements, form a metastable, non-close-packed hexagonal ω phase upon rapidly cooling from the high temperature single β phase field followed by isothermal annealing [1]. The ω phase has been actively studied for over 50 years due to its complex formation mechanism and its influence on mechanical and superconducting properties [2–5]. It is now widely accepted that athermal ω precipitates retain the composition of the parent β matrix and have been postulated to form by a purely displacive collapse of the {111} planes of the bcc phase via a shuffle mechanism [6,7]. In contrast, the isothermal ω precipitates have been postulated to form via a thermally activated process involving diffusion-based compositional partitioning followed by the collapse of {111} bcc planes in the compositionally depleted regions [6,7].

In this Letter, we present the salient aspects of the newly proposed transformation mechanism using titanium-molybdenum (Ti-Mo) alloys as a model system. Experiments reveal concurrent compositional and structural

instabilities within the undercooled bcc β phase of a Ti-Mo alloy leading to the formation of embryos with partially transformed ω-like structures. Nanometer-scale molybdenum-depleted pockets, arising from the early stages of phase separation (clustering) within the β matrix, have been qualitatively detected by using aberration-corrected high-resolution scanning transmission electron microscopy (HRSTEM) and quantitatively measured by three-dimensional atom probe (3DAP). Concurrent structural instabilities cause partial collapse of $\{111\}_\beta$ planes within these Mo-depleted pockets, leading to the formation of embryonic ω-like structures directly imaged at atomic resolution by using HRSTEM. Finally, first-principles electronic-structure calculations reveal that these partially transformed ω-like structures correspond to local energy minima in the free energy landscape, are composition-dependent, and lie between parent β and fully transformed ω phases.

Samples of forged and annealed Ti-9 at. % Mo (18 wt % Mo) alloy from the TIMETAL^{TM} company were solution heat-treated in the single β phase field at 1273 K for 30 min in a vacuum furnace ($\sim 1 \times 10^{-6}$ torr) and then rapidly cooled at $\sim 10\,^{\circ}\mathrm{C}/\mathrm{sec}$ in Ar gas. Some of these rapidly cooled samples were subsequently annealed at 748 K for 30 min. Microscopy specimens were prepared by using the FEI Nova Nanolab 200 dual-beam focused ion beam system and characterized by using a FEI Titan 80–300 TEM and in a local electrode atom probe (LEAP^{TM}) system from Cameca Instruments Inc. [8]. The LEAP samples were run in electric-field evaporation mode at 70 K, with an evaporation rate of 0.2%–1.0% and a voltage pulse fraction at 20% of the steady-state applied voltage. TEM studies of atomic-resolution Z-contrast imaging [through high angle annular dark field (HAADF)-HRSTEM] was performed at 300 kV by using a Corrected Electron Optical Systems probe aberration corrector.

Well-developed 30–50 nm sized ω precipitates (not shown) have been observed in the Ti-9 at. % Mo sample that was β solutionized (at 1273 K), quenched, and then isothermally annealed for 30 min at 748 K. The displacement of atomic columns within the bcc phase, equivalent to the collapse of the $\{111\}\beta$ planes, leading to the formation of the ω phase is illustrated by the schematic β motif in Fig. 1(a) and has been discussed in the literature [1,6,7]. This fully developed ω structure is clearly visible in the atomic-resolution TEM image shown in Fig. 1(b) from the 748 K annealed Ti-9 at. % Mo sample. The same sample has also been analyzed by using a 3D atom probe, and a tomographic reconstruction of the ω precipitates, defined by a 93 at. % Ti-rich isoconcentration surface, together with Mo atoms in red is shown as an inset in Fig. 1(c) [9]. The compositional partitioning of Mo across the β-ω interface is also shown as a proxigram analysis using ten ω precipitates, calculated with a bin size of 0.1 nm [10]. The large difference between the Mo contents of the β ($\sim$12 at. %) and the ω ($\sim$3.5 at. %) regions in this image

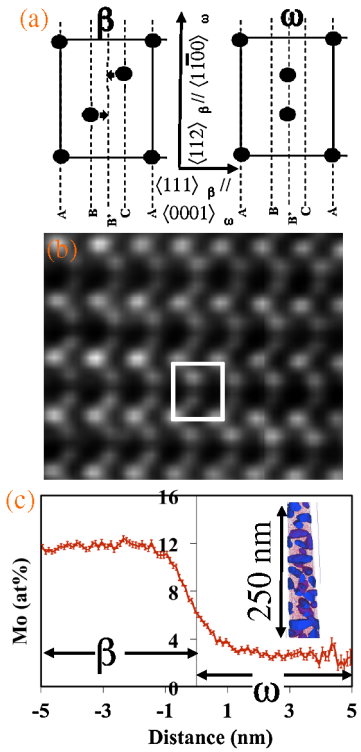

FIG. 1 (color online). (a) Schematic arrangement of atoms as seen from the $\langle 110\rangle\beta$ zone axis, corresponding to the β and fully collapsed ω motifs. Small arrows show the shifts of atoms along $\langle 111\rangle\beta$ directions. (b) HRTEM image recorded along the $\langle 011\rangle\beta$ zone axis, in a 748 K/30 min aged Ti-9 at. % Mo sample, showing the collapse in atomic columns corresponding to the well-developed ω phase. (c) Proximity histogram using Ti = 93 at. % isosurface that shows substantial compositional partitioning between the β and ω phases. The inset shows the corresponding 3DAP reconstruction of the Ti-rich regions.

indicates substantial rejection of Mo from the growing ω precipitates during isothermal annealing at 748 K.

A filtered high-resolution HAADF-STEM image from the rapidly cooled Ti-9 at. % Mo sample, viewed along the $\langle 011\rangle$ direction of the β matrix is shown in Fig. 2(a). This HAADF-STEM image exhibits regions of relatively brighter and darker contrast indicative of differences in atomic masses between these regions (Z contrast). In some cases the darker regions of lower Z exhibit shifts in the atomic columns corresponding to the nanoscale embryos of the ω-like phase. Two such ω-like embryos are marked in Fig. 2(a). Figure 2(b) is an atom probe reconstruction depicting Ti-rich regions as an isoconcentration surface (Ti = 93 at. %) together with the corresponding proximity histogram showing Mo partitioning across this interface with $\sim$6 at. % and $\sim$10 at. % Mo in the solute-depleted and solute-rich regions, respectively [10].

Figure 3(a) is an enlarged HAADF-HRSTEM image showing the undisplaced and partially displaced atom columns representing the β matrix and an ω-like embryo, respectively. The partially collapsed $\{111\}$ planes of the bcc (β) matrix are evident within the ω-like embryo in the

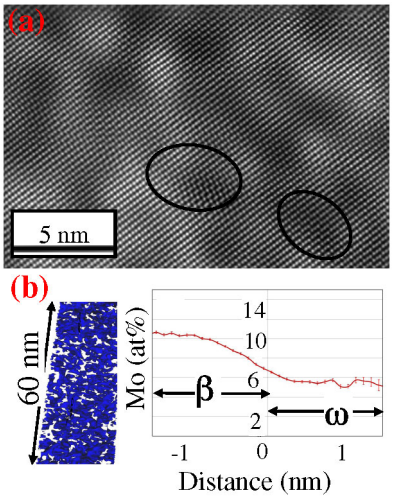

FIG. 2 (color online). (a) Filtered HAADF-HRSTEM image of rapidly cooled Ti-9 at. % Mo sample recorded along the $\langle 011\rangle\beta$ zone axis showing the atomic columns within the bcc matrix as well as marked ω embryo regions. (b) 3DAP atomic reconstruction of Ti-rich regions as isoconcentration surfaces (Ti = 93 at. %). The corresponding proximity histogram shows the compositions of solute-rich and solute-lean regions.

supercell. In Fig. 3(b), we quantify the atomic displacements within the ω-like embryo with respect to the β matrix by plotting the column intensities along rows 1, 2, and 3 as a function of distance along $\langle 111\rangle$ beta direction. For simplicity, the origin for each row has been transposed to overlap, and the structure transitions from β to ω-like as we move from left to right along the distance axis. The spacing between adjacent atomic columns along row 1 is $3d_{222}$, where d_{222} is the interplanar spacing between the {222} planes of the β structure. The collapse of the {111} planes can be described as a displacement wave of wavelength $\lambda = 3d_{222}$ and a corresponding wave vector of $2/3\langle 111\rangle^*$ (reciprocal space) [11,12]. Based on this formalism, complete β to ω transformation corresponds to a longitudinal displacement wave of $0.5d_{222}$ amplitude. As seen in Fig. 3(b), the displacements of the atomic columns in rows 2 and 3 are in the range $0.16d_{222}$–$0.2d_{222}$, progressively increasing on moving from left to right along the distance axis in Fig. 3(b) (from β to ω region). Consequently, the partial collapse of the {111} planes, observed here, indicates a smaller amplitude of the displacement wave compared to that seen in full collapse. This is further illustrated by crystal motifs in Fig. 3(b) depicting B and C planes forming a partially collapsed ω-like structure.

Density functional theory calculations.—Systems with 0, 8.33, and 16.66 at. % Mo in Ti were studied. Molybdenum atoms were added on collapsing {111} planes of β and ω titanium and these structures relaxed by using Vienna *ab initio* simulation package (VASP) [13–15] and projector augmented wave pseudopotentials [16]. The generalized gradient approximation of Perdew, Burke, and Ernzerhof was used [17]. A plane-wave kinetic-energy cutoff of 400 eV and $3 \times 3 \times 5$ k-point mesh size was used to ensure an accuracy of 1 meV/atom. For titanium we treat the $3p$ states as valence states in addition to the usual $4s$ and $3d$ states to increase accuracy. Nudged elastic band calculations [18] with constant cell volume yield the minimum energy pathway for the β to ω transformation shown in Fig. 4(a). The dependence of results on system size was examined by studying systems with 12, 24, and 48 atoms in the supercell, and energy barriers are accurate to about 2 meV/atom. While there is no activation barrier for β to ω transformation in the pure Ti system, we see a local energy minimum for the Ti-8.3 at. % Mo system along the minimum energy pathway corresponding to an average partial collapse of (222) planes. The normalized interplanar spacing for this local minimum structure is 0.25 from nudged elastic band calculations, in agreement with the experimental value of 0.20. Interestingly, $\langle 111\rangle$ atom columns with a Mo atom do not collapse while a neighboring parallel $\langle 111\rangle$ column with Ti does so. Such a partially collapsed structure is energetically favored over a fully collapsed structure when we have Mo atoms in the cell. For full collapse to occur, Mo atoms must diffuse out of the omega region.

We propose the following mechanism for the formation of embryonic ω within the β matrix. An undercooled alloy of composition Ti-9 at. % Mo presumably has a free energy lying within the miscibility gap (also within the spinodal)

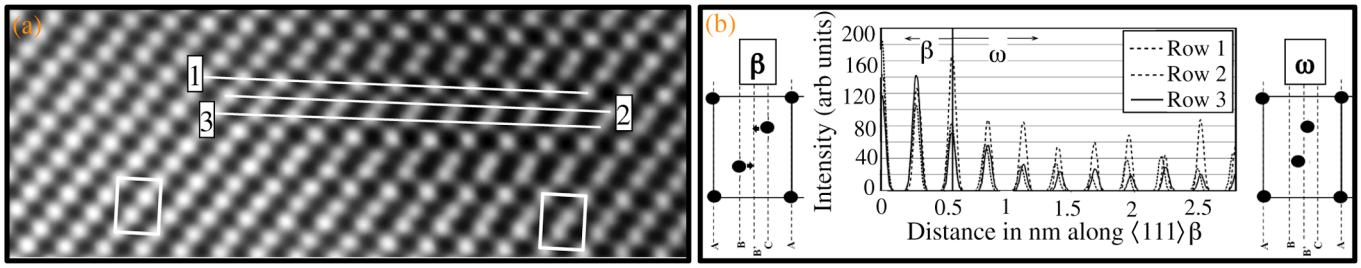

FIG. 3 (color online). (a) Enlarged HAADF-HRSTEM image of rapidly cooled Ti-9 at. % Mo sample showing the undisplaced and partially displaced atomic columns within the β matrix and ω embryo, respectively. In (a), three consecutive $\langle 111\rangle\beta$ columns have been marked to calculate the atomic displacements. (b) The plot in the center shows the column intensities along rows 1, 2, and 3 [as shown in (a)] as a function of distance along $\langle 111\rangle\beta$ directions. On both sides of the plot, cartoons show the arrangement of atoms as seen from the $\langle 110\rangle\beta$ zone axis, along with the β and partially collapsed ω motifs.

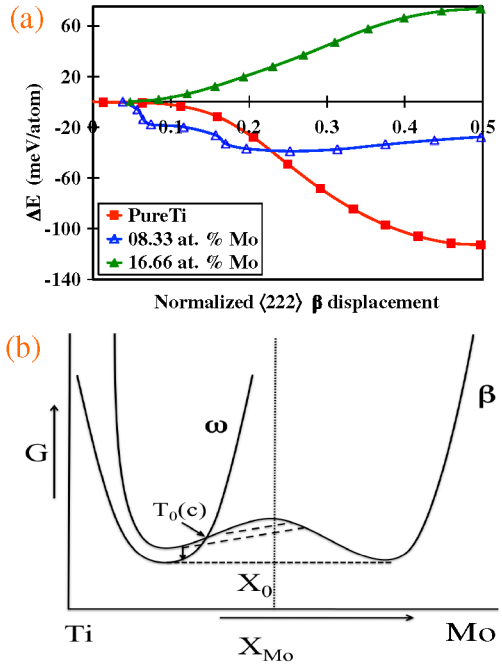

FIG. 4 (color online). (a) Nudged elastic band plots of the relative system energy ΔE along the minimum energy path with β taken as a reference for 24 atom systems with 0, 8.33, and 16.66 at. % Mo in Ti. (b) A schematic plot of Gibbs free energy versus composition.

of the β phase as shown for the composition marked X_0 in Fig. 4(b) and, consequently, is unstable with respect to compositional fluctuations. This leads to nanoscale, compositional clustering (phase separation) into *Mo-enriched* and *Mo-depleted* regions, presumably by a spinodal decomposition process as indicated by the dotted lines in Fig. 4(b). As compositional fluctuations grow in amplitude and wavelength, the solute (Mo) depleted regions within the β phase cross the $T_0(c)$ point of intersection of the β and ω free energy curves. These solute-depleted regions now become metastable (or unstable) with respect to the structural instability causing partial collapse of the {111} β planes and the formation of ω-like embryos. Subsequent diffusional rejection of Mo from the growing embryos leads to an increase in the degree of collapse of {111} bcc planes eventually forming a fully developed hexagonal ω structure. Systematic density-functional theory calculations to correlate local atomic displacements and composition of solute-depleted regions in Ti-Mo alloys are currently underway.

Summary.—By coupling aberration-corrected HAADF-STEM with atom probe tomography and density-functional theory calculations, the early stages of phase separation (compositional clustering) and consequent displacive collapse of {111} bcc planes within the solute-depleted regions of the β matrix of Ti-Mo alloys have been established. These results provide novel insights into the mechanisms of solid-state transformations in metallic systems by capturing the earliest stages of nucleation at atomic to near atomic spatial and compositional resolution. To the best of our knowledge, this is the first clear experimental evidence, corroborated by first-principles calculations, of a close coupling between the composition and displacive component associated with product phase embryos in a first-order mixed-mode transformation. We believe that this mechanism is broadly relevant to many materials.

The National Science Foundation (Grants No. 6701956, No. 0700828, and No. 0846444) and U.S. Air Force Research Laboratory ISES contract funded this work. Experimental facilities at UNT's Center for Advanced Research and Technology and OSU's Center for the Accelerated Maturation of Materials and the Talon Linux cluster at UNT were used.

*srinivasan.srivilliputhur@unt.edu
†banerjee@unt.edu

[1] S. Banerjee and P. Mukhopadhyay, *Phase Transformations—Examples from Ti and Zr Alloys* (Pergamon, Oxford, 2007).
[2] P. D. Frost, W. M. Parris, L. L. Hirsch, J. R. Doig, and C. M. Schwartz, Trans. Am. Soc. Met. **46**, 231 (1954).
[3] R. R. Boyer, G. Welsch, amd E. W. Collings, *Materials Properties Handbook: Ti Alloys* (American Society for Metals, Metals Park, OH, 1994).
[4] I. Bakonyi, H. Ebert, and A. I. Liechtenstein, Phys. Rev. B **48**, 7841 (1993).
[5] G. B. Grad, P. Blaha, J. Luitz, and K. Schwarz, Phys. Rev. B **62**, 12 743 (2000).
[6] D. D. Fontaine, N. E. Paton, and J. C. Williams, Acta Metall. **19**, 1153 (1971).
[7] J. C. Williams, D. D. Fontaine, and N. E. Paton, Metall. Mater. Trans. B **4**, 2701 (1973).
[8] M. K. Miller, K. F. Russell, K. Thompson, R. Alvis, and D. J. Larson, Microsc. Microanal. **13**, 428 (2007).
[9] A. Devaraj, R. E. A. Williams, S. Nag, R. Srinivasan, H. L. Fraser, and R. Banerjee, Scr. Mater. **61**, 701 (2009).
[10] O. C. Hellman, J. A. Vandenbroucke, J. Rusing, D. Isheim, and D. N. Seidman, Microsc. Microanal. **6**, 437 (2000).
[11] D. D. Fontaine, Acta Metall. **18**, 275 (1970).
[12] D. D. Fontaine and O. Buck, Philos. Mag. **27**, 967 (1973).
[13] G. Kresse and J. Hafner, Phys. Rev. B **47**, 558 (1993).
[14] G. Kresse and J. Hafner, Phys. Rev. B **49**, 14 251 (1994).
[15] G. Kresse and D. Joubert, Phys. Rev. B **59**, 1758 (1999).
[16] P. E. Blöchl, Phys. Rev. B **50**, 17 953 (1994).
[17] J. P. Perdew, K. Burke, and M. Ernzerhof, Phys. Rev. Lett. **78**, 1396 (1997).
[18] H. Jònsson, G. Mills, and K. Jacobsen, *Classical and Quantum Dynamics in Condensed Phase Simulations* (World Scientific, Singapore, 1998), 1st ed.